energies

Article

A Novel Semianalytical Model for the Relationship between Formation Pressure and Water Saturation in Coalbed Methane Reservoirs

Long Yang [1], Yizhong Zhang [1,2,*], Maolin Zhang [1,2] and Bin Ju [3]

[1] School of Petroleum Engineering, Yangtze University, Wuhan 430113, China; yanglong_ytze@163.com (L.Y.); zmlmhy65@126.com (M.Z.)
[2] Cooperative Innovation Center of Unconventional Oil and Gas, Yangtze University, Wuhan 430113, China
[3] School of Oil and Gas Engineering, Southwest Petroleum University, Chengdu 610500, China; bc_j2009@foxmail.com
* Correspondence: yizhongzhang@yangtzeu.edu.cn

Abstract: The accuracy of the relationship between formation pressure and water saturation has a direct impact on predicting the production performance of coal reservoirs. As a result, researchers are becoming more interested in this connection. The most commonly used method to evaluate this connection is the semianalytic method, but it disregards the impact of coal matrix shrinkage on pore compressibility, resulting in inaccurate water saturation estimations for coal reservoirs. A material balance equation that considers the effect of coal matrix shrinkage on cleat porosity and pore compressibility, as well as the gas–water relative permeability curve, is used for the first time in this study to establish a model between pressure and water saturation. Furthermore, this study extends the proposed pressure–saturation model to predict cumulative gas production and gas recovery, resolving the difficult problem of calculating recovery for coalbed methane reservoirs. To verify its accuracy, this study compares the proposed method with numerical simulations and previous methods; the results of the comparison show that the water saturation under formation pressure calculated by the method proposed in this study is closer to the results of the numerical simulation. Sun's model ignores the effect of matrix shrinkage on pore compressibility, resulting in larger calculation results. The findings of this study indicate that the effect of coal matrix shrinkage on pore compressibility cannot be ignored, and that the proposed method can replace numerical simulation as a simple and accurate method for water saturation evaluation, which can be applied to predict cumulative gas and recovery estimation for closed coalbed methane reservoirs. The proposed method increases the accuracy of the semianalytical method and broadens its application. It is critical for the prediction of coal reservoir production performance and forecasting of production dynamics.

Keywords: coalbed methane reservoirs; formation pressure and water saturation; pore compressibility; recovery; material balance

Citation: Yang, L.; Zhang, Y.; Zhang, M.; Ju, B. A Novel Semianalytical Model for the Relationship between Formation Pressure and Water Saturation in Coalbed Methane Reservoirs. *Energies* **2023**, *16*, 875. https://doi.org/10.3390/en16020875

Academic Editors: Jie Zhu and Bo Wang

Received: 7 November 2022
Revised: 6 January 2023
Accepted: 9 January 2023
Published: 12 January 2023

1. Introduction

When conventional energy sources become scarce, unconventional energy sources gain popularity due to their abundant reserves [1–3]. Coalbed methane reservoirs, unlike conventional gas reservoirs, are thought of as dual pore media (matrix and cleat), with the matrix serving as storage space and the cleat serving as flow channels. The exploitation of coalbed methane is complicated due to the unique characteristics of coal reservoirs [4,5]. There are three stages to the exploitation of coalbed methane (CBM) reservoirs [6]. In the first stage, the formation pressure is higher than the critical desorption pressure; the adsorbed gas in the matrix cannot be desorbed, resulting in no gas diffusion into the cleat, low gas saturation in the cleat, and poor gas flow ability. In the second stage, the formation pressure is lower than the critical desorption pressure, and the adsorbed gas in the matrix begins to desorb and diffuse into the cleat. Because of the low initial gas saturation and poor mobility, gas accumulates in the cleat pores, causing a rapid decrease in water saturation. In the third stage, the adsorbed gas is desorbed, more gas diffuses into the cleat, previously isolated bubbles connect, and the gas within the cleat is produced and has mobility, resulting in a slower decrease in water saturation. The assessment of formation pressure and water saturation in CBM reservoirs is complex due to the uniqueness of CBM extraction, but the relationship between pressure and water saturation is critical to the prediction of production dynamics in CBM wells. The connection has a significant impact on the establishment of flowing material balance (FMB) of gas and water in CBM reservoirs [7,8]. The connection can be used to calculate the desorption area of a CBM reservoir [9–11]. It is crucial for evaluating the effective permeability of the gas/water phase [12], and can also be used to reliably estimate CBM well production [13,14]. Furthermore, the connection can be used to calculate recoverable reserves. This calculation completes the prediction of recovery and serves as a reference for well network deployment in the reservoir, which is useful for gas reservoir development design. As a result, it becomes critical to determine the precise connection between formation pressure and water saturation in coalbed methane reservoirs.

The numerical simulation, material balance, and semianalytical approaches are the three basic methodologies for characterizing the connection between formation pressure and water saturation in CBM reservoirs. To obtain the connection, the numerical simulation technique takes more data and more complicated simulations [15,16], making it difficult to employ in production situations. The material balance equation (MBE) can calculate historical average water saturation based on production dynamic data such as cumulative gas production (Gp), cumulative water production (Wp), and total reserves (G), but is less effective in predicting future water saturation [17–22]. The semianalytical method ignores the effect of matrix shrinkage on the calculation of CBM pore compressibility when the formation pressure is below the critical desorption pressure [6], which has a greater impact on CBM reservoirs with low cleat porosity and leads to inaccurate water saturation calculation results.

In this study, the semianalytical method was modified to calculate the connection between formation pressure and water saturation by considering the effect of matrix shrinkage on pore compressibility when the formation pressure is below the critical desorption pressure. The accuracy of the proposed method is demonstrated by comparing the results of numerical simulations with those of the proposed method in this study. This model compensates for flaws in previous approaches to determining the pressure–saturation connection in CBM reservoirs. It has wide application prospects because it can be applied to several aspects of CBM exploitation, including calculating recoverable reserves, calculating recovery, and providing guidance for well network deployment schemes.

Section 2.1 contains the model's assumptions, Section 2.2 contains the establishment of the pressure–saturation connection, Section 2.3 contains the application strategy of the proposed method, Section 3.1 contains the validation of the proposed method, Section 3.2 contains a sensitivity analysis of the critical parameters, Section 3.3 contains the application of the proposed method, Section 3.4 contains a discussion of positive and negative aspects of the proposed method, and Section 4 contains the conclusions.

2. Materials and Methods

2.1. Model Assumptions

The model proposed in this study is applicable to evaluate the connection between the formation pressure and water saturation of CBM reservoirs. There are several assumptions: (1) The two-phase flow of gas and water within the cleat follows Darcy's law, ignoring the effects of gravity and capillary. (2) The CBM adsorption model is Langmuir isotherm adsorption. (3) The CBM reservoir is a closed gas reservoir. (4) Dissolved gas in water is not considered. (5) The adsorbed gas within the matrix is transferred to the cleat by diffusion.

2.2. The Connection between Formation Pressure and Water Saturation

During extraction, the CBM in the formation mainly contains two parts (adsorbed gas and free gas). Therefore, the total remaining gas reserves can be expressed as:

$$G = G_{mp} + G_{ap} \tag{1}$$

Usually, the volumetric method is used to calculate the remaining reserves of free gas [23], and the calculation formula is as follows:

$$G_{mp} = \frac{A_s h \phi (1 - s_w)}{B_g} \tag{2}$$

The change in pore volume can be divided into two parts. When the formation pressure is above the critical desorption pressure, the pore volume change is primarily influenced by stress sensitivity, whereas when the formation pressure is below the critical desorption pressure, the pore volume change is primarily influenced by both matrix shrinkage and stress sensitivity [24–26]. It is advised that the pore compressibility should be calculated considering not only stress sensitivity but also matrix shrinkage.

When the formation pressure is higher than the critical desorption pressure [27], the cleat porosity can be calculated by Equation (3) as follows.

$$\phi = \phi_i [1 - c_m (p_i - p)] \tag{3}$$

When the formation pressure is below the critical desorption pressure [24], the cleat porosity can be calculated using the following formula.

$$\phi = \phi_i \left[1 - c_m (p_i - p) + \frac{1}{\phi_i} \left(\frac{K_b}{M_b} - 1 \right) (eps - eps0) \right] \tag{4}$$

$$eps(p) = \frac{\varepsilon_L p}{p_L + p} \tag{5}$$

Define the following expression:

$$c_a = -\frac{\varepsilon_L}{\phi_i} \left(\frac{K_b}{M_b} - 1 \right) \tag{6}$$

Substituting Equations (5) and (6) into Equations (3) and (4), the following equations can be obtained:

$$\phi = \phi_i f(p) \tag{7}$$

$$f(p) = \begin{cases} 1 - c_m (p_i - p) & p \geq p_d \\ 1 - c_m (p_i - p) + c_a \left(\frac{p_d}{p_L + p_d} - \frac{p}{p_L + p} \right) & p < p_d \end{cases} \tag{8}$$

The Langmuir adsorption isotherm [28] is used to calculate the content of adsorbed gas, and the remaining reserves of adsorbed gas can be expressed as:

$$G_{ap} = A_s h V_E(p) \tag{9}$$

The adsorbed gas is not desorbed when the formation pressure is higher than the critical desorption pressure. It begins to desorb when the formation pressure is lower than the critical desorption pressure [9].

$$V_E(p) = \begin{cases} \dfrac{V_L p_d}{p_L + p_d} & p \geq p_d \\ \dfrac{V_L p}{p_L + p} & p < p_d \end{cases} \tag{10}$$

Substituting Equations (2), (7), and (9) into Equation (1), the total remaining gas reserves can be obtained:

$$G = A_s h \left(\frac{\phi_i f(p)(1 - s_w)}{B_g} + V_E(p) \right) \tag{11}$$

Taking the derivative of Equation (11) with respect to the pressure, the following expressions can be obtained:

$$\frac{\partial G}{\partial p} = A_s h \phi_i \left[\frac{\left(f'(p)(1-s_w) - f(p)\frac{\partial s_w}{\partial p} \right) B_g - f(p)(1-s_w) B_g{}'}{\left(B_g\right)^2} + \frac{V_E{}'(p)}{\phi_i} \right] \tag{12}$$

In the same way, the volumetric method can be used to calculate the remaining reserves of water [29]. The expression is as follows:

$$N_w = \frac{A_s h \phi s_w}{B_w} \tag{13}$$

Taking the derivative of Equation (13) with respect to the pressure, the following expressions can be obtained:

$$\frac{\partial N_w}{\partial p} = A_s h \phi_i \frac{\left(f'(p) s_w + f(p)\frac{\partial s_w}{\partial p} \right) B_w - f(p) s_w B_w'}{\left(B_w\right)^2} \tag{14}$$

The gas–oil production ratio can be expressed as the ratio of cumulative gas production to cumulative oil production under instantaneous pressure changes. Therefore, the gas–water ratio of production can be expressed as:

$$R_{gw} = \frac{\partial G / \partial p}{\partial N_w / \partial p} = \frac{\frac{\left[\begin{array}{l} \left(f'(p)(1-s_w) - f(p)\frac{\partial s_w}{\partial p} \right) B_g \\ -f(p)(1-s_w) B_g{}' \end{array} \right]}{\left(B_g\right)^2} + \frac{f(p) V_E{}'(p)}{\phi}}{\frac{\left(f'(p) s_w + f(p)\frac{\partial s_w}{\partial p} \right) B_w - f(p) s_w B_w'}{\left(B_w\right)^2}} \tag{15}$$

From the definition of the compressibility of free gas, the compressibility of water, and the compressibility of adsorbed gas, the following expression can be obtained:

$$c_g = -\frac{1}{V_{fg}} \left(\frac{\partial V_{fg}}{\partial p} \right) = -\frac{1}{V_{fg}/V_{sg}} \left(\frac{\partial \left(V_{fg}/V_{sg} \right)}{\partial p} \right) = -\frac{1}{B_g} \left(\frac{\partial B_g}{\partial p} \right) \tag{16}$$

$$c_w = -\frac{1}{V_{fw}} \left(\frac{\partial V_{fw}}{\partial p} \right) = -\frac{1}{V_{fw}/V_{sw}} \left(\frac{\partial \left(V_{fw}/V_{sw} \right)}{\partial p} \right) = -\frac{1}{B_w} \left(\frac{\partial B_w}{\partial p} \right) \tag{17}$$

$$c_d = \frac{B_g V_E{}'(p)}{\phi} = \begin{cases} 0 & p \geq p_d \\ \dfrac{V_L p_L B_g}{\left(p_L + p\right)^2 \phi} & p < p_d \end{cases} \tag{18}$$

Considering the shrinkage effect of the coal matrix when the adsorbed gas begins to desorb, redefining the pore compressibility according to Equation (7), the following expression can be obtained:

$$c_p = \frac{1}{\phi}\frac{\partial \phi}{\partial p} = \frac{f'(p)}{f(p)} = \begin{cases} \dfrac{c_m}{1 - c_m(p_i - p)} & p \geq p_d \\ \dfrac{c_m - \frac{c_a p_L}{(p_L + p)^2}}{1 - c_m(p_i - p) + c_a\left(\dfrac{p_d}{p_L + p_d} - \frac{p}{p_L + p} \right)} & p < p_d \end{cases} \tag{19}$$

Substituting Equations (16)–(19) into Equation (15), the following expressions can be obtained:

$$\begin{aligned} R_{gw} = \frac{\partial G/\partial p}{\partial N_w/\partial p} &= \frac{\dfrac{f(p)\left[c_p(1-s_w) - \dfrac{\partial s_w}{\partial p}\right] + f(p)\left[(1-s_w)c_g + c_d\right]}{B_g}}{\dfrac{f(p)\left(c_p s_w + \dfrac{\partial s_w}{\partial p}\right) + f(p) s_w c_w}{B_w}} \\ &= \frac{\left[c_p(1-s_w) - \dfrac{\partial s_w}{\partial p}\right] + \left[(1-s_w)c_g + c_d\right]}{\left(c_p s_w + \dfrac{\partial s_w}{\partial p}\right) + s_w c_w} \frac{B_w}{B_g} \end{aligned} \tag{20}$$

The gas–water flow follows Darcy's seepage, so the gas–water production expression is:

$$q_g = \frac{2\pi\alpha r K K_{rg} h}{\mu_g B_g} \frac{\partial p}{\partial r} \tag{21}$$

$$q_w = \frac{2\pi\alpha r K K_{rw} h}{\mu_w B_w} \frac{\partial p}{\partial r} \tag{22}$$

The gas–water ratio of production can also be expressed as:

$$R_{gw} = \frac{q_g}{q_w} = \frac{B_w}{B_g} \frac{K_{rg}}{K_{rw}} \frac{\mu_w}{\mu_g} \tag{23}$$

Combining Equation (20) and Equation (23), the following expression can be obtained:

$$\frac{\left[c_p(1-s_w) - \frac{\partial s_w}{\partial p}\right] + \left[(1-s_w)c_g + c_d\right]}{\left(c_p s_w + \frac{\partial s_w}{\partial p}\right) + s_w c_w} = \frac{K_{rg}}{K_{rw}} \frac{\mu_w}{\mu_g} \tag{24}$$

According to the definition of the mobility ratio of water and gas, the following expression can be obtained:

$$M = \frac{K_{rw}}{K_{rg}} \frac{\mu_g}{\mu_w} \tag{25}$$

Substituting Equation (25) into Equation (24), the following expression can be obtained:

$$\frac{\left[c_p(1-s_w) - \frac{\partial s_w}{\partial p}\right] + \left[(1-s_w)c_g + c_d\right]}{\left(c_p s_w + \frac{\partial s_w}{\partial p}\right) + s_w c_w} = \frac{1}{M} \tag{26}$$

Arranging Equation (26), the following formula can be obtained:

$$s_w\left[\left(c_p + c_w\right) + M\left(c_p + c_g\right)\right] + \frac{\partial s_w}{\partial p}(1+M) = M\left(c_p + c_g + c_d\right) \tag{27}$$

Define the following expression:

$$\begin{aligned} &A = M\left(c_p + c_g + c_d\right) \\ &B = c_p + c_w + M\left(c_p + c_g\right) \\ &C = M + 1 \end{aligned} \tag{28}$$

Substituting Equation (28) into Equation (27), the following equation can be obtained:

$$C\frac{\partial s_w}{\partial p} + B s_w = A \tag{29}$$

2.3. Calculation Strategies of the Connection between Formation Pressure and Water Saturation

If we consider the pressure divided into small interval segments, A, B, and C can be regarded as constants. Solving Equation (29), the general solutions can be obtained:

$$s_w = \frac{A}{B} - \frac{D}{B} e^{-\frac{B}{C} p} \tag{30}$$

D is a constant in the general solution. At the current moment, the water saturation can be represented as:

$$s_w^n = \frac{A}{B} - \frac{D}{B} e^{-\frac{B}{C} p^n} \tag{31}$$

At the next moment, the water saturation can be represented as:

$$s_w^{n+1} = \frac{A}{B} - \frac{D}{B} e^{-\frac{B}{C} p^{n+1}} \tag{32}$$

Substituting Equation (31) into Equation (32), the following expression can be obtained:

$$s_w^{n+1} = \frac{A}{B} - \left(\frac{A}{B} - s_w^n \right) e^{\frac{B}{C} (p^n - p^{n+1})} \tag{33}$$

To calculate the mobility ratio of water and gas, it is necessary to obtain the relative permeability of gas to water. The Corey equation is usually used to characterize the gas–water relative permeability curve, and the expression is as follows [30]:

$$K_{rg} = K_{rg\max} (1 - s_w^*)^{n_g} \tag{34}$$

$$s_w^* = \frac{s_w - s_{wc}}{1 - s_{wc}} \tag{35}$$

$$K_{rw} = (s_w^*)^{n_w} \tag{36}$$

From Equation (33), in order to evaluate the relationship between pressure and water saturation, the mobility ratio of water and gas needs to be determined. However, it can be seen from Equation (25) that calculating the mobility ratio of water and gas requires specifying the relative permeability of gas and water. It is also known from Equations (34)–(36) that the calculation of the relative permeability requires the clarification of the water saturation. Therefore, to calculate the relationship between pressure and water saturation, an iterative algorithm should be used. In a closed CBM reservoir, water is not replenished as extraction proceeds, so the relationship between water saturation and pressure possesses monotonicity and can be solved iteratively using the dichotomous method. The calculation strategy for the proposed method is as follows:

(1) Regress the experimental data of relative permeability to obtain the constant n_g and n_w of the Corey equation.
(2) Get the formation pressure (p^n) and water saturation (s_w^n) at the current moment.
(3) Define $a = s_{wc}$, $b = s_{wi}$.
(4) Assume the water saturation $s_{wa} = \frac{a+b}{2}$ at the next moment.
(5) Calculate the gas relative (K_{rg}^{n+1}) permeability using Equation (34) and the water relative permeability (K_{rw}^{n+1}) using Equation (36) at the next moment.
(6) Calculate the pressure ($p^{n+1} = p^n - \Delta p$) at the next moment. In this study, $\Delta p = 0.1$ MPa is assumed.
(7) Calculate the compressibility of the pore (c_p) using Equation (19), the compressibility of adsorbed gas (c_d) using Equation (18), and the mobility ratio of water and gas (M) using Equation (25).
(8) Calculate the value of A, B, and C using Equation (28) at the next moment.
(9) The saturation (s_w^{n+1}) at the next moment can be calculated using Equation (33).
(10) If the calculated $s_w^{n+1} > s_{wa}$, assign $a = s_{wa}$; if the calculated $s_w^{n+1} \leq s_{wa}$, assign $b = s_{wa}$.

(11) Calculate the error ($error = abs\left(s_w^{n+1} - s_{wa}\right)$) between the calculated water saturation (s_w^{n+1}) and the assumed water saturation (s_{wa}).
(12) Calculate the interval ($E = abs(a - b)$) between a and b.
(13) If the current interval (E) is less than the minimum interval (eps), or the current error ($error$) is less than the minimum error (err), the saturation under the formation pressure p^{n+1} can be accepted as s_w^{n+1}. Otherwise, return to step (4) and continue the calculation until the requirements are met. The steps are shown in Figure 1.

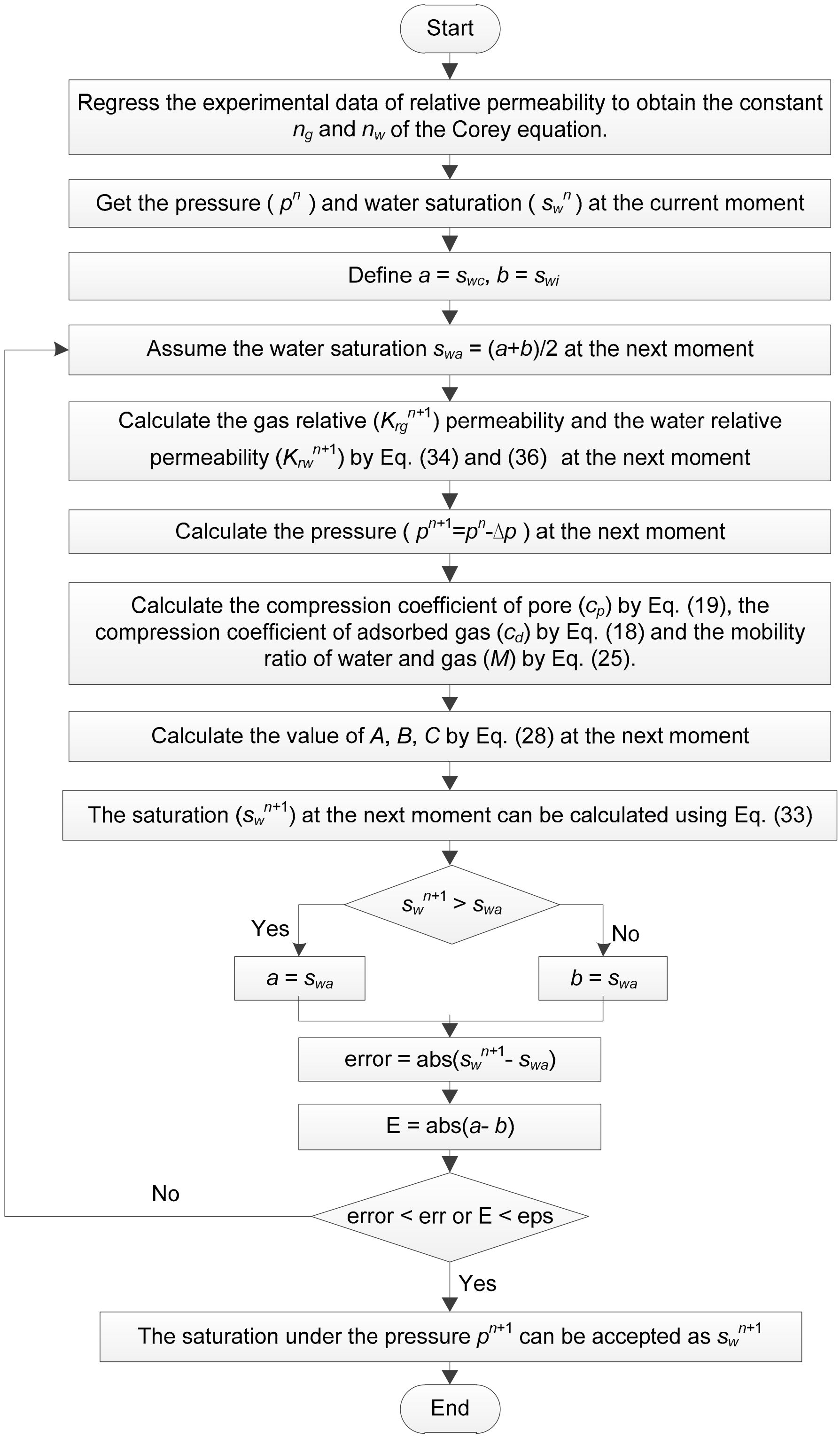

Figure 1. Calculation flowchart of the connection between pressure and saturation.

3. Results and Discussion

3.1. Validation of the Proposed Method

Due to the lack of test data on formation pressure and water saturation for the CBM reservoir under production conditions, a numerical simulation case is used in this study to verify the accuracy of the proposed method. The Schlumberger Eclipse numerical simulation software is widely used and accepted for simulating coalbed methane extraction. In this study, Eclipse is used to demonstrate the precision of the proposed formation pressure and water saturation relationship model for coalbed methane reservoirs. This proposed model is compared with a numerical simulation (Schlumberger Eclipse E100) and with Sun's approach [6]. The number of grids of the numerical simulation model is 31 in the X-direction, 31 in the Y-direction, and 2 in the Z-direction. The permeability of the numerical simulation model in the X-, Y-, and Z-directions is 10 mD. The grid size of the numerical simulation model is 100 m in the X-direction, 100 m in the Y-direction, and 10 m in the Z-direction. The depths of the top face of the grid block are 1200 m. The numerical simulation model considers only the permeability of the cleat, and the desorbed gas in the matrix is transferred into the cleat by diffusion. The detailed parameters used in the numerical simulation model are listed in Table 1. The gas Z-factor and viscosity employed in the model are depicted in Figure 2, and the adsorption gas concentrations employed are shown in Figure 3.

Table 1. The parameters used in the numerical simulation.

Parameters	Values	Parameters	Values
s_{wi}, fraction	0.95	s_{wc}, fraction	0.25
V_L, m^3/m^3	27.63	K_{rgmax}	1
p_L, MPa	3.10	n_g	2.5
ϕ_i, fraction	0.001	n_w	2.5
p_i, MPa	20	B_w, m^3/m^3	1.01
c_m, MPa^{-1}	0.00051	μ_w, mPa·s	0.36
c_w, MPa^{-1}	0.00051	K_b, MPa	67,400
ε_L	0.015	Temperature, °C	80.0
p_d, MPa	15	M_b, MPa	88,800
DX	31	*DY*	31
DZ	2	*DXV*, m	100
DYV, m	100	*DZV*, m	10
Kx, mD	10	*Ky*, mD	10
Kz, mD	10	*DH*, m	1200

Based on the above data, the connection between formation pressure and water saturation of the CBM reservoir can be calculated using the method proposed in this study and Sun's method; the comparison results are shown in Figure 4. It is evident that the connection between formation pressure and water saturation calculated by the proposed method is nearly identical to that of the numerical simulation. As the formation pressure decreases, the amount of CBM desorption becomes larger, and the coal matrix shrinkage has a greater effect on the pore compressibility. Sun's method, without correction for the pore compressibility, has an increasing deviation from the numerical simulation. This result implies that the connection between formation pressure and water saturation of the CBM reservoir calculated by the method proposed in this study is more accurate compared with previous methods. The model proposed in this study can replace numerical simulation as a simple and reliable method for evaluating the water saturation under the formation pressure of CBM reservoirs.

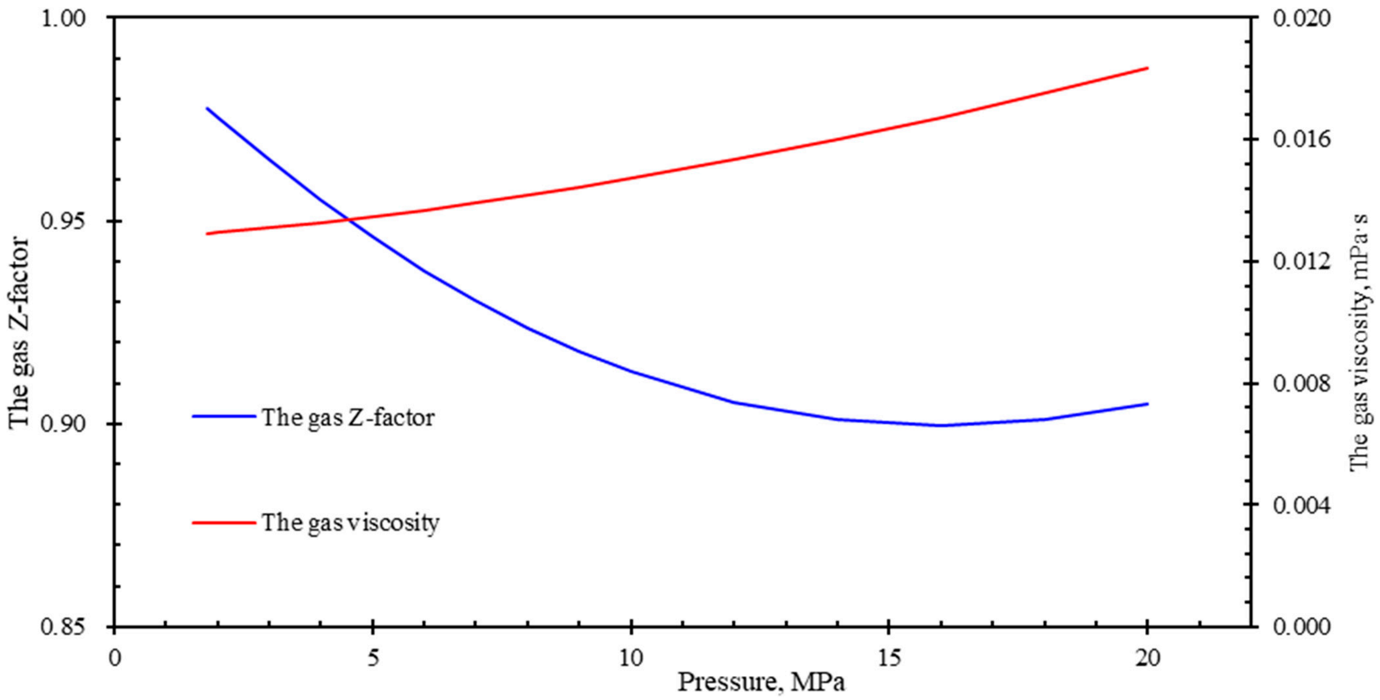

Figure 2. Gas Z-factor and viscosity used in the numerical simulation model.

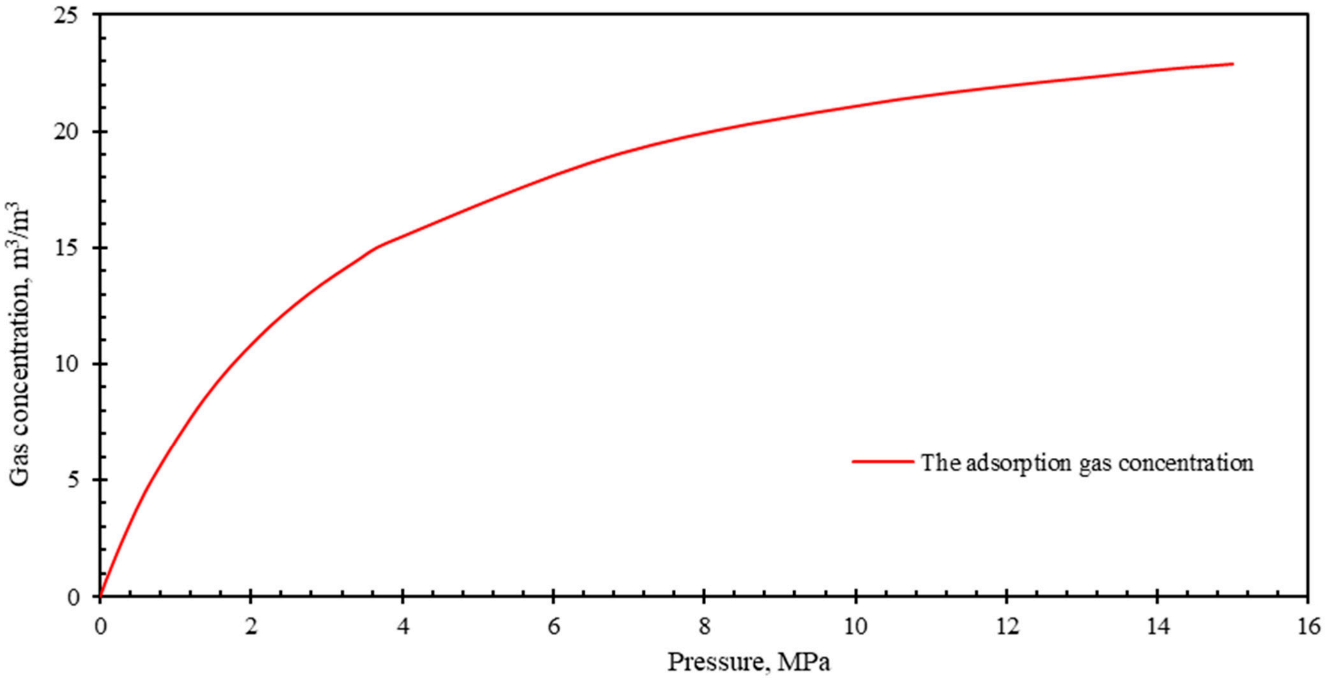

Figure 3. Adsorption gas concentration used in the numerical simulation model.

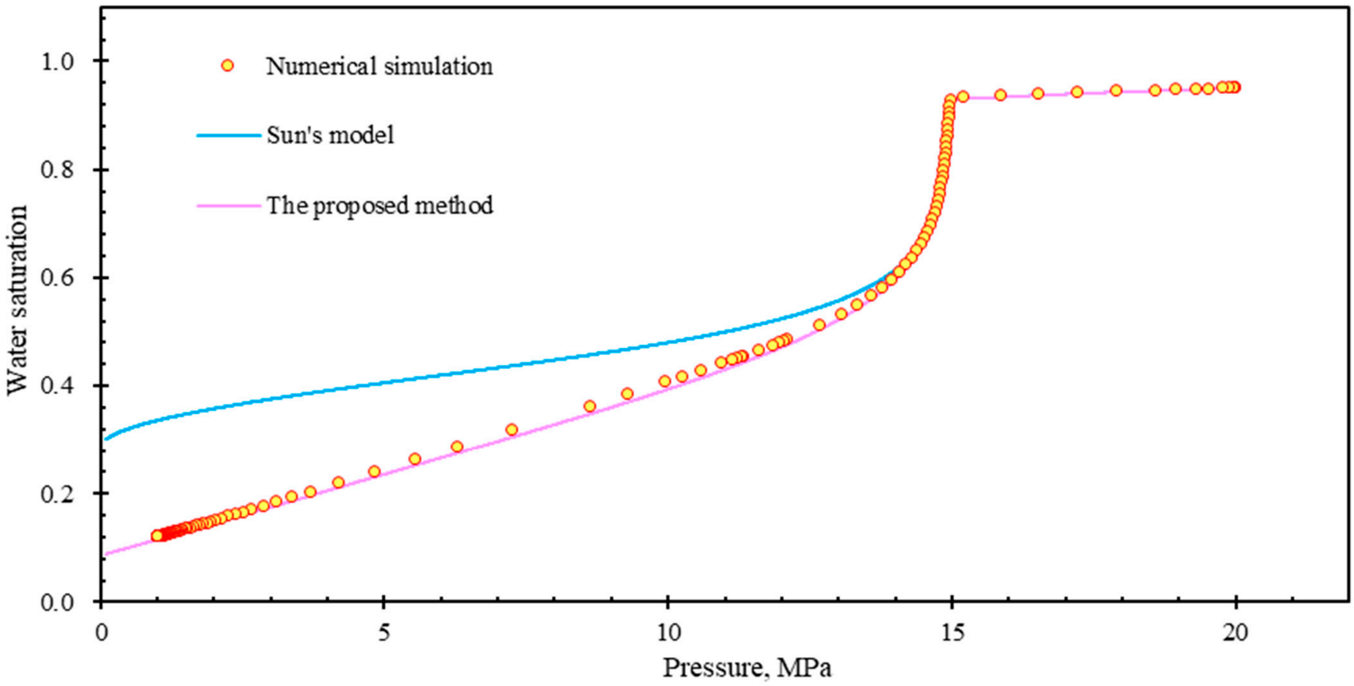

Figure 4. Comparison results of the proposed method with the numerical simulation method and Sun's method.

3.2. The Sensitivity Analysis of Critical Factors

According to Equations (33) and (28), the compressibility of the pore (c_p), the compressibility of the adsorbed gas (c_d), and the mobility ratio of water and gas (M) can influence the calculated results of water saturation at formation pressure. These parameters are calculated by the Langmuir volume (V_L), the Langmuir volumetric strain (ε_L), and the gas–water relative permeability. Therefore, the sensitivity of these critical factors is analyzed in this study by assuming different values.

The effect of Langmuir volume (V_L) on the results of water saturation calculations was verified by assuming different Langmuir volumes (V_L) using the parameters listed in Table 1, and the results are shown in Figure 5. It is evident from Figure 5 that because the adsorbed gas has not yet been desorbed, when the formation pressure is higher than the critical desorption pressure, the Langmuir volume does not affect the water saturation. When the formation pressure is lower than the critical desorption pressure, the larger the Langmuir volume, the larger the gas saturation in the pore and the higher the gas flow capacity. This is because the smaller the Langmuir volume, the less gas will be desorbed and diffuse into the cleat, resulting in higher water saturation.

From the literature [16,31–34], it is known that reasonable values of Langmuir volumetric strain (ε_L) are between 0.005 and 0.025. Therefore, to analyze their effects on water saturation, different Langmuir volumetric strains (ε_L) are assumed, and the results are shown in Figure 6. It can be seen from Figure 6 that when the formation pressure is lower than the critical desorption pressure, the greater the Langmuir volumetric strain, the greater the gas saturation, and the stronger the gas flow capacity. With the decrease of the formation pressure, the difference in water saturation calculated by different Langmuir volumetric strains becomes larger. This is because the larger the Langmuir volumetric strain, the greater the increase in cleat porosity from matrix shrinkage, and because the gas expands more easily than water, the saturation of gas will increase while the saturation of water will decrease.

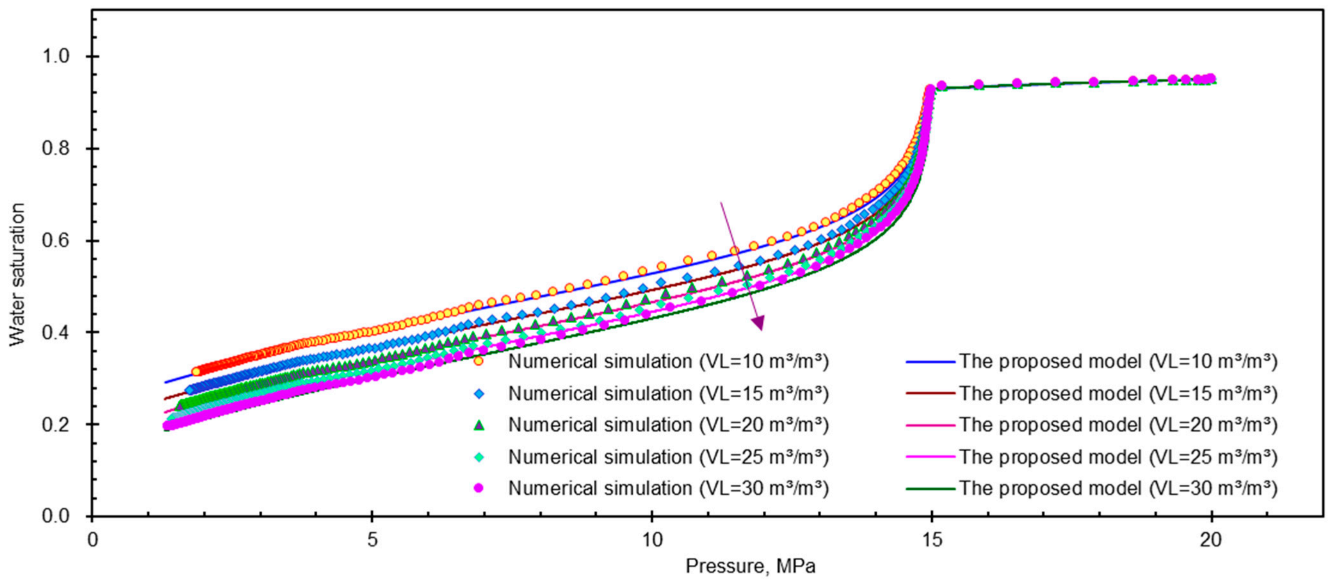

Figure 5. Comparison of calculation results of the proposed method considering different Langmuir volumes.

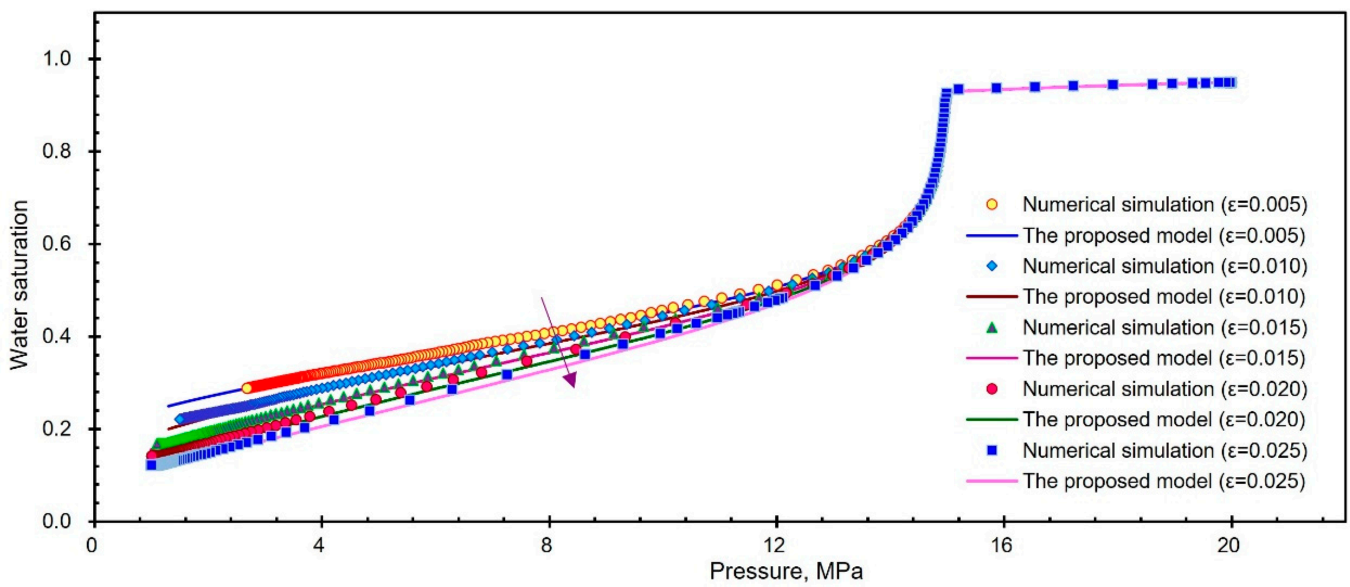

Figure 6. Comparison of calculation results of the proposed method considering different Langmuir volumetric strains.

Assuming different relative permeability curves as shown in Figure 7, the water saturation at different formation pressures was calculated using the data in Table 1 and the calculated results are compared as shown in Figure 8. It can be seen from Figure 8 that as the relative permeability of water increases and the relative permeability of gas decreases, water saturation becomes smaller. This is because as the relative permeability of water increases, water flow capacity and water production increase, leading to a reduction in the remaining amount of water in the pore, which in turn leads to a reduction in the saturation of the water. The difference in water saturation calculated by different relative permeability curves will increase first and then decrease with the decline of formation pressure, and finally the water saturation will converge. When the water saturation decreases until it is irreducible, only gas is involved in the flow of the CBM reservoir, and the water saturation in the pore will eventually converge, as illustrated by the water MBE. As a result, during the production process, the relative permeability of water should be increased in order to minimize water saturation and the influence of water on gas flow.

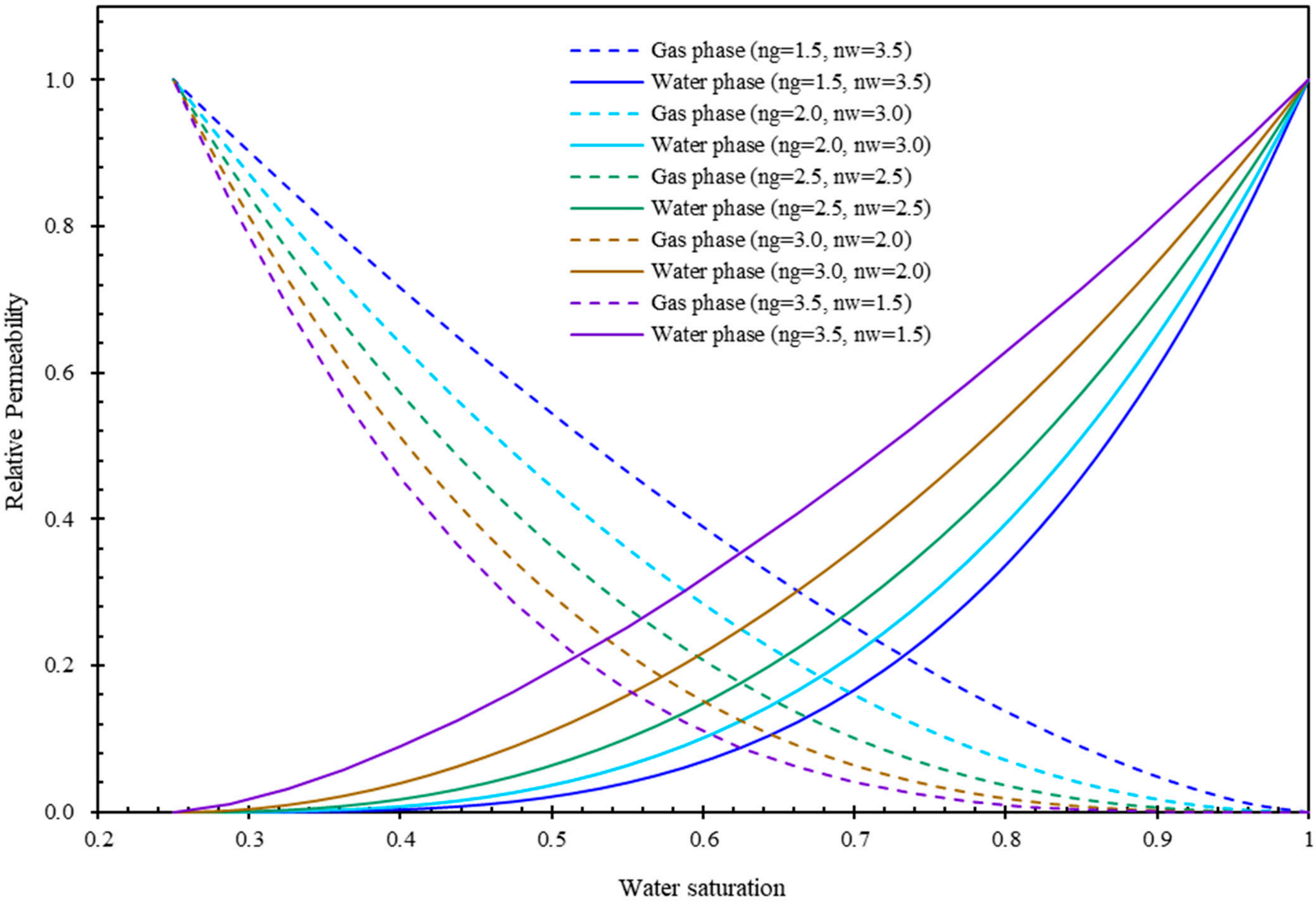

Figure 7. Different gas–water relative permeability curves.

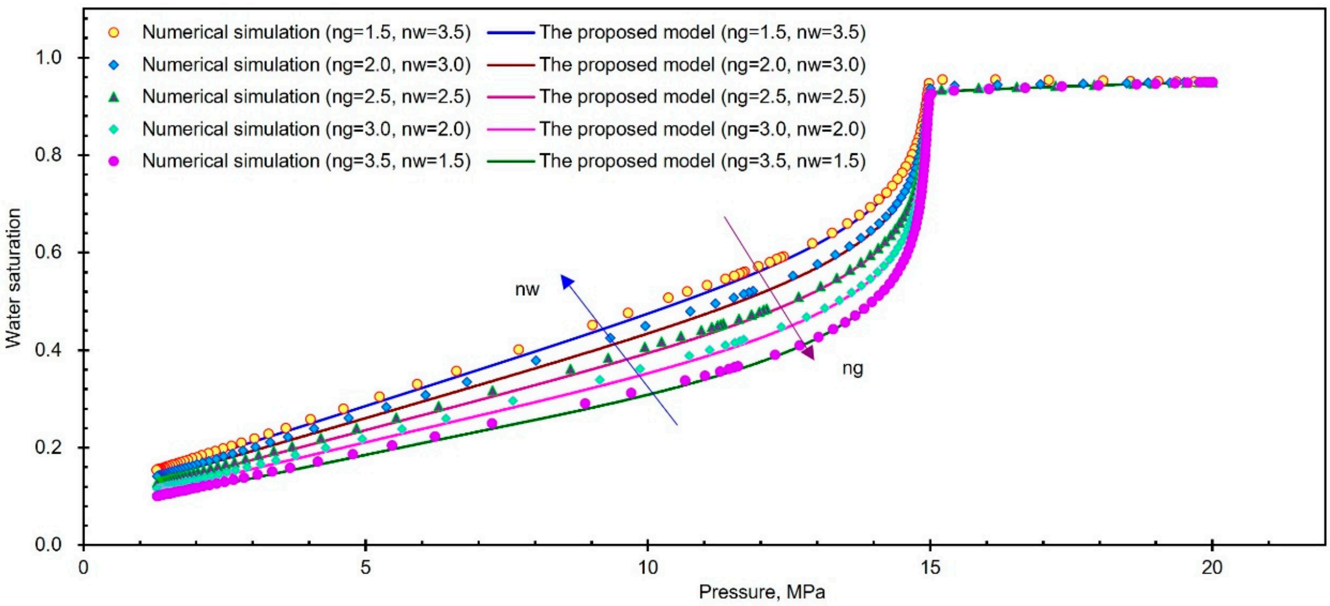

Figure 8. Comparison of calculation results of the proposed method considering different gas–water relative permeability curves.

3.3. Application of the Proposed Method

The pressure–saturation relationship can be applied to several aspects, including calculating the desorption area of CBM [9–11], establishing the gas/water FMB of CBM reservoirs [8], describing the connection between the formation pressure and effective permeability of CBM reservoirs [12], and accurately predicting the production rate of CBM reservoirs [14]. Furthermore, the proposed model can also predict the connection between formation pressure and cumulative production of a CBM reservoir, which can be used to evaluate the recoverable reserves of the reservoir. The method proposed in this study can also be combined with the MBE for CBM reservoirs in order to solve the difficult problem of recovery calculation, and to provide guidance for well network deployment.

Considering the MBE of water [23] and gas [27], the Wp and Gp of the CBM reservoir can be calculated as follows:

$$W_p = \frac{A_s h \phi_i s_{wi} - A_s h \phi s_w + A_s h \phi_i s_{wi} c_w (p_i - p)}{B_w} \tag{37}$$

$$G_p = A_s h \left[\frac{\phi_i (1 - s_{\mathrm{wi}})}{B_{gi}} - \frac{\phi (1 - s_w)}{B_g} \right] + A_s h [V_E(p_d) - V_E(p)] \tag{38}$$

Using the method of calculating formation pressure and water saturation proposed in this study, and according to Equation (37) and Equation (38), the Wp and Gp can be calculated. The calculated results of the applied model were compared with the results of the numerical simulation, as shown in Figures 9 and 10. The average relative deviation of the predicted Gp from the numerical simulation is 0.05%, while the average relative deviation of the predicted Wp from the numerical simulation is 3.64%. The relative deviations are extremely small, reflecting the fact that the Wp and Gp calculated in this study are consistent with the numerical simulation.

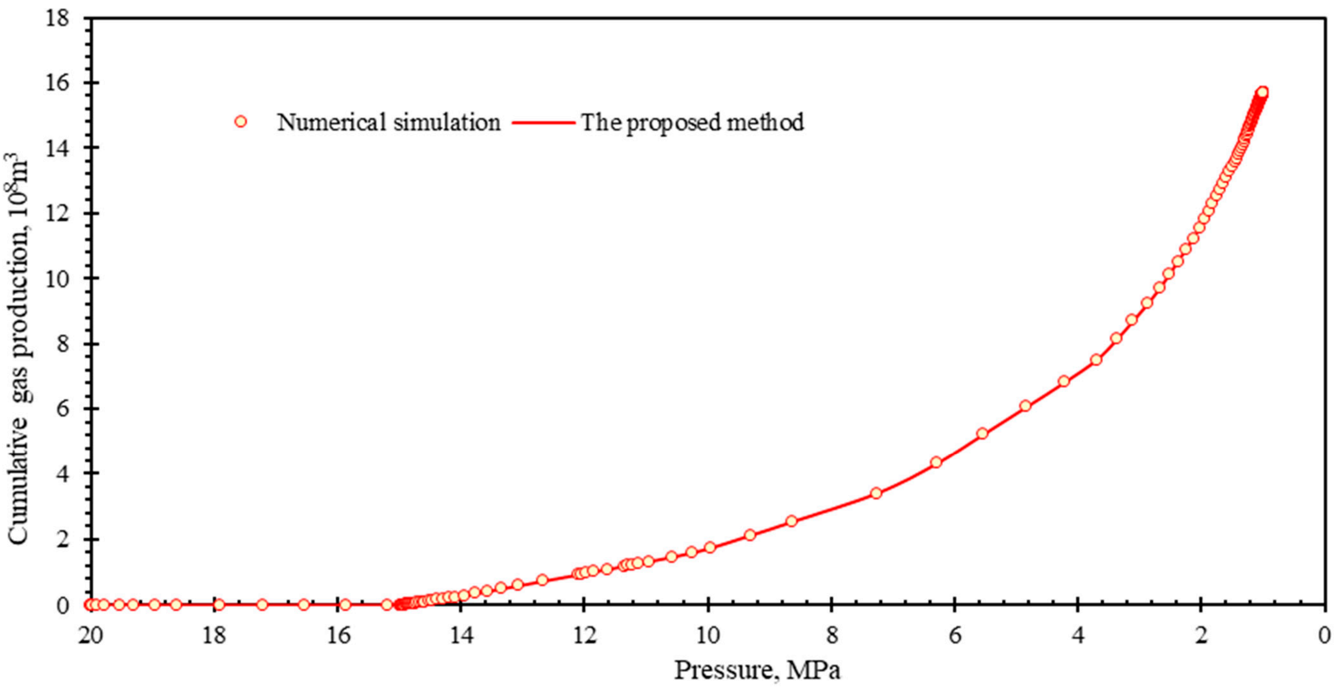

Figure 9. Comparison results of cumulative gas production with numerical simulation.

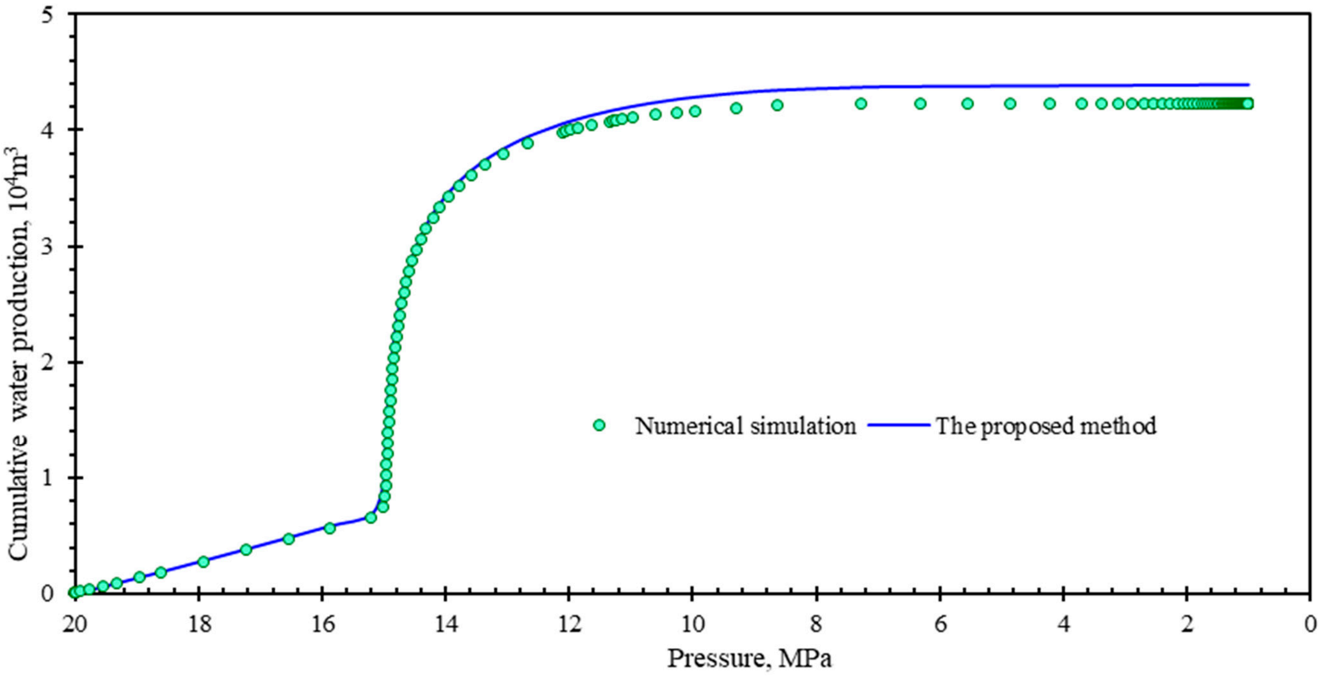

Figure 10. Comparison results of cumulative water production with numerical simulation.

The corresponding Wp and Gp at different formation pressures can be obtained using the method proposed in this study. Furthermore, the recoverable reserves and recovery under abandonment pressure can be calculated according to Equation (39), and the results of comparing the method proposed in this study with the results of numerical simulations are displayed in Table 2.

$$E_R = \frac{G_{pr}}{G_i} \tag{39}$$

Table 2. Comparison of recoverable reserves and recovery predicted by the proposed method with numerical simulation results.

Methods	Recoverable Coalbed Methane Reserves (10^8 m^3)	Recovery %
Numerical simulation	13.42	60.88
Proposed method	13.41	60.83
Relative Deviation, %	0.07	0.07

Note: The abandoned pressure is 1.5 MPa.

As shown in Table 2, the difference between the calculation results of the proposed method and the numerical simulation is small, with a recovery deviation of only 0.07% at the abandoned formation pressure of 1.5 MPa. This demonstrates that the method proposed in this study is extremely effective at predicting recovery. Based on the calculated recoverable reserves and recovery, a reasonably efficient well network and well spacing can be deployed, and a reasonable development plan can be formulated to maximize economic benefits for the CBM reservoir.

3.4. Discussion

The relationship between the formation pressure and water saturation of a CBM reservoir is modeled in this paper from the standpoint of material conservation. The effect of matrix shrinkage on the pore compressibility is thought to compensate for previous models' shortcomings. The benefits of this model include fewer parameters, a simple calculation process, and accurate calculation results. It can be used to calculate the effective permeability of CBM reservoirs, desorption area, establish a FMB equation of CBM wells, predict production dynamics of CBM wells, predict recoverable reserves of CBM reservoirs, and guide well network deployment of CBM reservoirs. However, the model still has some flaws. For example, it can only be applied to closed coal reservoirs without taking into account external water intrusion, and it can only be applied to gas reservoirs with depleted extraction. This application premise limits the types of scenarios in which the model can be used. As a result, in future research, external water intrusion and other types of mining methods, such as gas injection and water injection mining, should be considered in order to expand the model's application scenarios.

4. Conclusions

In this study, a model of the connection between formation pressure and water saturation of the CBM reservoir was proposed; unlike previous models, this model considers the effect of coal matrix shrinkage on pore compressibility. The calculated results are compared with numerical simulations, and the following conclusions can be drawn.

(1) A model for calculating the connection between formation pressure and water saturation in CBM reservoirs, considering the effect of coal matrix shrinkage on the cleat porosity and pore compressibility, is established. Compared with previous models, the calculation results of the proposed model are closer to numerical simulations, makes up for the shortcomings of previous methods, and can replace numerical simulation as a simple and accurate evaluation method for the relationship between pressure and water saturation in CBM reservoirs.
(2) When the formation pressure is lower than the critical desorption pressure, with the increase of Langmuir volume or Langmuir volume strain, the water saturation becomes smaller, and the gas seepage ability becomes stronger; as the relative permeability of water increases or the relative permeability of gas decreases, the water saturation decreases.
(3) The method proposed in this study can be used to complete the calculation of recoverable reserves of coalbed methane reservoirs and to evaluate their recovery, which is critical for the development of CBM well network deployment schemes.

Author Contributions: L.Y.: Methodology; Y.Z.: Conceptualization; M.Z.: Supervision; B.J.: Data curation. All authors have read and agreed to the published version of the manuscript.

Funding: This research was funded by National Natural Science Foundation of China grant number 52004032.

Data Availability Statement: The data presented in this study are available on request from the corresponding author.

Acknowledgments: The authors would like to acknowledge the support from the School of Petroleum Engineering at Yangtze University.

Conflicts of Interest: The authors declare that they have no known competing financial interests or personal relationships that could have appeared to influence the work reported in this paper.

Nomenclature

G	remaining total gas reserves of coalbed methane, m^3
G_{mp}	remaining free gas reserves of coalbed methane, m^3
G_{ap}	remaining adsorbed gas reserves of coalbed methane, m^3
A_s	area, m^2
h	thickness, m
ϕ	cleat porosity of coalbed methane reservoirs, fraction
s_w	water saturation, fraction
B_g	volume factor of the gas, m^3/m^3
c_m	compressibility of the rock, MPa^{-1}
p	formation pressure, MPa

p_i	initial formation pressure, MPa
ϕ_i	initial cleat porosity of coalbed methane reservoirs, fraction
K_b	bulk modulus, MPa
M_b	constrained axial modulus, MPa
$eps(p)$	strain term, dimensionless
$eps0$	initial strain term, dimensionless
ε_L	Langmuir volumetric strain, dimensionless
p_L	Langmuir pressure, MPa
c_a	coal matrix shrinkage compressibility, dimensionless
$f(p)$	the variation coefficient of cleat porosity, fraction
p_d	critical desorption pressure, MPa
$V_E(p)$	amount of adsorption per unit volume, m^3/m^3
V_L	Langmuir volume, m^3/m^3
N_w	water reserves of coalbed methane reservoirs, m^3
B_w	volume factor of water, m^3/m^3
R_{gw}	gas–water ratio, m^3/m^3
c_g	compressibility of gas, MPa^{-1}
c_w	compressibility of water, MPa^{-1}
c_d	compressibility of desorption, MPa^{-1}
V_{fg}	volume of gas in the formation, m^3
V_{sg}	volume of gas under the standard conditions, m^3
V_{fw}	volume of water in the formation, m^3
V_{sw}	volume of water under the standard conditions, m^3
c_p	comprehensive compressibility of pore, MPa^{-1}
r	control radius of a single well, m
K	absolute permeability, D
μ_g	viscosity of gas, mPa·s
μ_w	viscosity of water, mPa·s
q_g	gas production rate, m^3/d
q_w	water production rate, m^3/d
K_{rg}	relative permeability of gas, dimensionless
K_{rw}	relative permeability of water, dimensionless
M	mobility ratio of water and gas, dimensionless
$K_{rg\max}$	maximum relative permeability of gas, dimensionless
s_{wc}	irreducible water saturation, fraction
n_w	Corey's constant of the water phase
n_g	Corey's constant of gas phase
Δp	pressure interval, MPa
s_{wa}	assumed water saturation, fraction
W_p	cumulative water production, m^3
G_{pr}	recoverable reserves, m^3
G_p	cumulative gas production, m^3
G_i	total gas reserves of coalbed methane, m^3
E_R	recovery, fraction
DX	number of grids in the X-direction
DY	number of grids in the Y-direction
DZ	number of grids in the Z-direction
DXV	grid size in X-direction, m
DYV	grid size in Y-direction, m
DZV	grid size in Z-direction, m
Kx	absolute permeability in the X direction, mD
Ky	absolute permeability in the Y direction, mD
Kz	absolute permeability in the Z direction, mD
DH	depths of the top face of the grid block, m

Superscript	
n	the current moment
n + 1	the next moment
Constant	
α	86.4

References

1. Bao, Y.; Wei, C.; Neupane, B. Generation and accumulation characteristics of mixed coalbed methane controlled by tectonic evolution in Liulin CBM field, eastern Ordos Basin, China. *J. Nat. Gas Sci. Eng.* **2016**, *28*, 262–270. [CrossRef]
2. Wu, K.; Chen, Z.; Li, X.; Xu, J.; Li, J.; Wang, K.; Dong, X. Flow behavior of gas confined in nanoporous shale at high pressure: Real gas effect. *Fuel* **2017**, *205*, 173–183. [CrossRef]
3. Zhang, Y.; Ju, B.; Zhang, M.; Wang, C.; Zeng, F.; Hu, R.; Yang, L. The effect of salt precipitation on the petrophysical properties and the adsorption capacity of shale matrix based on the porous structure reconstruction. *Fuel* **2022**, *310*, 122287. [CrossRef]
4. Kazanin, O.I.; Meshkov, A.A.; Sidorenko, A.A. Prospects for development of a techno-logical structure of underground coal mines. *MIAB. Min. Inf. Anal. Bull* **2022**, *6*, 35–53.
5. Sidorenko, A.A.; Meshkov, S.A. Justification of technologies parameters for intensive mining of prone to spontane-ous combustion thick coal seams. *MIAB Min. Inf. Anal. Bull* **2022**, *6*, 83–99.
6. Sun, Z.; Li, X.; Shi, J.; Zhang, T.; Feng, D.; Sun, F.; Li, L. A semi-analytical model for the relationship between pressure and saturation in the cbm reservoirs. *J. Nat. Gas Ence Eng.* **2018**, *49*, 365–375. [CrossRef]
7. Clarkson, C.R.; Salmachi, A. Rate-transient analysis of an undersaturated CBM reservoir in Australia: Accounting for effective permeability changes above and below desorption pressure. *J. Nat. Gas Sci. Eng.* **2017**, *40*, 51–60. [CrossRef]
8. Sun, Z.; Shi, J.; Zhang, T.; Wu, K.; Miao, Y.; Feng, D.; Li, X. The modified gas-water two phase version flowing material balance equation for low permeability CBM reservoirs. *J. Pet. Sci. Eng.* **2018**, *165*, 726–735. [CrossRef]
9. Xu, B.; Li, X.; Haghighi, M.; Du, X.; Yang, X.; Chen, D.; Zhai, Y. An analytical model for desorption area in coal-bed methane production wells. *Fuel* **2013**, *106*, 766–772. [CrossRef]
10. Sun, Z.; Li, X.; Shi, J.; Yu, P.; Huang, L.; Xia, J.; Feng, D. A semi-analytical model for drainage and desorption area expansion during coal-bed methane production. *Fuel* **2017**, *204*, 214–226. [CrossRef]
11. Sun, Z.; Shi, J.; Wu, K.; Liu, W.; Wang, S.; Li, X. A prediction model for desorption area propagation of coalbed methane wells with hydraulic fracturing. *J. Pet. Sci. Eng.* **2019**, *175*, 286–293. [CrossRef]
12. Sun, Z.; Shi, J.; Zhang, T.; Wu, K.; Feng, D.; Sun, F.; Hou, C.; Li, X. A fully-coupled semi-analytical model for effective gas/water phase permeability during coal-bed methane production. *Fuel* **2018**, *223*, 44–52. [CrossRef]
13. Clarkson, C.R.; Qanbari, F. A semi-analytical method for forecasting wells completed in low permeability, undersaturated CBM reservoirs. *J. Nat. Gas Sci. Eng.* **2016**, *30*, 19–27. [CrossRef]
14. Sun, Z.; Shi, J.; Wang, K.; Miao, Y.; Zhang, T.; Feng, D.; Sun, F.; Wang, S.; Han, S.; Li, X. The gas-water two phase flow behavior in low-permeability CBM reservoirs with multiple mechanisms coupling. *J. Nat. Gas Sci. Eng.* **2018**, *52*, 82–93. [CrossRef]
15. Gentzis, T.; Bolen, D. The use of numerical simulation in predicting coalbed methane producibility from the Gates coals, Alberta Inner Foothills, Canada: Comparison with Mannville coal CBM production in the Alberta Syncline. *Int. J. Coal Geol.* **2008**, *74*, 215–236. [CrossRef]
16. Wu, K.; Chen, Z.; Li, X.; Dong, X. Methane storage in nanoporous material at supercritical temperature over a wide range of pressures. *Sci. Rep.* **2016**, *6*, 33461. [CrossRef]
17. King, G.R. Material balance techniques for coal seam and Devonian shale gas reservoirs. In Proceedings of the SPE Annual Technical Conference and Exhibition OnePetro, New Orleans, LA, USA, 23–26 September 1990.
18. King, G.R. Material-balance techniques for coal-seam and devonian shale gas reservoirs with limited water influx. *SPE Reserv. Eng.* **1993**, *8*, 67–72. [CrossRef]
19. Penuela, G.; Ordonez, A.; Bejarano, A. A generalized material balance equation for coal seam gas reservoirs. In Proceedings of the SPE Annual Technical Conference and Exhibition OnePetro, New Orleans, LA, USA, 27–30 September 1998.
20. Ahmed, T.H.; Centilmen, A.; Roux, B.P. A generalized material balance equation for coalbed methane reservoirs. In Proceedings of the SPE Annual Technical Conference and Exhibition OnePetro, San Antonio, TX, USA, 24–27 September 2006.
21. Firanda, E. The development of material balance equations for coalbed methane reservoirs. In Proceedings of the SPE Asia Pacific Oil and Gas Conference and Exhibition OnePetro, Jakarta, Indonesia, 20–22 September 2011.
22. Thararoop, P.; Karpyn, Z.T.; Ertekin, T. Development of a material balance equation for coalbed methane reservoirs accounting for the presence of water in the coal matrix and coal shrinkage and swelling. *J. Unconv. Oil Gas Resour.* **2015**, *9*, 153–162. [CrossRef]
23. Shi, J.; Chang, Y.; Wu, S.; Xiong, X.; Liu, C.; Feng, K. Development of material balance equations for coalbed methane reservoirs considering dewatering process, gas solubility, pore compressibility and matrix shrinkage. *Int. J. Coal Geol.* **2018**, *195*, 200–216. [CrossRef]
24. Palmer, I.; Mansoori, J. How permeability depends on stress and pore pressure in coalbeds. A new model. In Proceedings of the SPE Annual Technical conference and Exhibition OnePetro, Denver, Colorado, USA, 6–9 October 1996.
25. Harpalani, S.; Schraufnagel, R.A. Shrinkage of coal matrix with release of gas and its impact on permeability of coal. *Fuel* **1990**, *69*, 551–556. [CrossRef]

26. Ibrahim, A.F.; Nasr-El-Din, H.A. A comprehensive model to history match and predict gas/water production from coal seams. *Int. J. Coal Geol.* **2015**, *146*, 79–90. [CrossRef]
27. Sun, Z.; Wu, K.; Shi, J.; Li, Y.; Jin, T.; Li, Q.; Li, X. Novel prediction methods for under-saturated coalbed methane wells: Effect of drainage schedules. *J. Pet. Sci. Eng.* **2019**, *181*, 106215. [CrossRef]
28. Langmuir, I. The constitution and fundamental properties of solids and liquids. *Part, I. Solids. J. Am. Chem. Soc.* **1916**, *38*, 2221–2295. [CrossRef]
29. Shi, J.; Wu, J.; Lv, M.; Li, Q.; Liu, C.; Zhang, T.; Sun, Z.; He, M.; Li, X. A new straight-line reserve evaluation method for water bearing gas reservoirs with high water production rate. *J. Pet. Sci. Eng.* **2021**, *196*, 107808. [CrossRef]
30. Li, Y.; Li, X.; Teng, S.; Xu, D. Improved models to predict gas–water relative permeability in fractures and porous media. *J. Nat. Gas Sci. Eng.* **2014**, *19*, 190–201. [CrossRef]
31. Liu, T.; Liu, S.; Lin, B.; Fu, X.; Zhu, C.; Yang, W.; Zhao, Y. Stress response during in-situ gas depletion and its impact on permeability and stability of CBM reservoir. *Fuel* **2020**, *266*, 117083. [CrossRef]
32. Liu, A.; Liu, S.; Liu, P.; Harpalani, S. The role of sorption-induced coal matrix shrinkage on permeability and stress evolutions under replicated in situ condition for CBM reservoirs. *Fuel* **2021**, *294*, 120530. [CrossRef]
33. Shi, J.Q.; Durucan, S. Drawdown induced changes in permeability of coalbeds. A new interpretation of the reservoir response to primary recovery. *Transp. Porous Media* **2004**, *56*, 1–16. [CrossRef]
34. Wei, M.; Liu, C.; Liu, Y.; Liu, J.; Elsworth, D.; Tivane, O.A.; Li, C. Long-term effect of desorption-induced matrix shrinkage on the evolution of coal permeability during coalbed methane production. *J. Pet. Sci. Eng.* **2022**, *208*, 109378. [CrossRef]